# Photonic properties of multicontinuous cubic phases

V. Babin,[1] P. Garstecki,[1,*] and R. Hołyst[1,2]
[1]*Institute of Physical Chemistry PAS Department III, Kasprzaka 44/52, 01224 Warsaw, Poland*
[2]*WMP-SNS, Cardinal Stefan Wyszyński University Dewajtis 5, Warsaw, Poland*
(Received 16 August 2002; published 31 December 2002)

We present a systematic study of the photonic properties (band structures) of periodic multicontinuous cubic phases based on the *P*, *D*, *G*, *I-WP*, *F-RD*, and *C*(*P*) triply periodic minimal surfaces. We investigate the structures with up to five separate interwoven subvolumes. The influence of the dielectric constant modulation at different spatial scales is discussed. The lowest dielectric constant contrasts required to observe the full three-dimensional photonic band gaps are stated.

DOI: 10.1103/PhysRevB.66.235120 PACS number(s): 42.70.Qs

## I. INTRODUCTION

13 years have passed since the discovery[1,2] of the photonic band gap (PBG) materials—materials exhibiting a ''forbidden'' frequency region, where electromagnetic waves cannot propagate for both polarizations along any direction. From the very start the phenomena of controlling the flow of light without or with very minimal losses captured the imagination of many scientists. The effort to confirm the observations and to develop better PBG structures resulted in an exponentially growing number of both theoretical and experimental studies. For example, the first theoretical works, concerning optical properties of spherical (colloidal) particles arranged in fcc and dfcc lattices,[3] has already been cited several hundred times.

The theoretical studies concentrate on solving Maxwell's equations (ME's) for a periodic dielectric medium (PDM). In the absence of nonlinear effects the possible forms of electromagnetic propagation can be expressed as superpositions of definite-frequency (time-harmonic) modes of ME's. Several approaches towards eigenmode decomposition of ME's in PDM have been proposed. The aim of a largest area of the theoretical studies is to find a structure which displays the widest possible full PBG.

On the other hand, experimental efforts are aimed at manufacturing materials of desired photonic properties. Here two main streams can be underlined. One is the so-called top-down approach in which sophisticated methods for engineering at the $\mu$ m level are used. Several periodic structures with very low defect density have been already manufactured.[4,5] However the top-down approach has some drawbacks such as a slow fabrication rate and usually high costs. An alternative is the bottom-up method which rely on self-assembly processes. It is often enough to mix the proper constituents to observe a self-assembly at nanoscale,[6] micron scale,[7] or macroscale.[8] The world of self-assembly is very rich. The phenomenon has been observed, studied and used in many different systems (surfactants,[9] polymers,[10] colloids,[11] etc.). Even though the defect density is still a problem there are already prominent examples of successful fabrication of large monocrystalline domains with interesting photonic properties.[12]

Self-assembly processes provide various geometries of the resultant periodic media. To our knowledge, within the structures accessible through the self-assembly, the widest full three-dimensional (3D) photonic gaps[13,14] are found in the triply periodic multicontinuous architectures (TPMCA's). A detailed explanation of the structure of these phases is contained in Sec. III. The first computations of the band structure $\omega_n(\mathbf{k})$ for the TPMCA were done for the special case of a two subvolume (2V) system with the interface given by a triply periodic minimal surface (TPMS). During our computations we became aware of another report[14] concerning photonic properties of these structures. In this report it has been shown that the 2V structures based on the double diamond (*D*) TPMS display a gap of a quality factor (QF) $f=100\Delta\omega/\omega_0$ up to 27 and the gyroid (*G*) TPMS based phases up to 24. However, (i) our calculations for the 2V structures provide slightly different results, (ii) Maldovan *et al.*[14] did not find any full 3D photonic gap in three subvolume systems which is in a disagreement with our results, and (iii) optical properties of multicontinuous *P*, *D*, *G* and some other well-known structures [*I-WP*,*F-RD*,*C*(*P*)] have not been examined.

The purpose of this work is to provide a detailed, systematic study of the photonic properties of multicontinuous (two, three, four and five subvolume) triply periodic structures. In addition to giving an exhaustive view of the photonic properties of the TPMCA we want to answer the following questions. (i) Does the low spatial scale modulation of the dielectric constant enhance the band gap widths similarly to the coated spherical particle systems? (ii) Does it induce opening of several gaps at different frequency scales?

Up to now the TPMCA architectures are most easily obtained in surfactant and polymer systems. In the amphiphilic mixtures both bicontinuous and tricontinuous cubic structures have been observed. In block copolymer systems the bicontinuous and tricontinuous phases have already been explored and there is no constraint prohibiting *n*-block copolymer to form even more complicated multicontinuous cubic phases. In order to use the multi continuous phase as a template for the photonic crystal, the blocks can be either selectively enriched in a polymerizing inorganic agent, or selectively etched and filled with a different material.

The frequency used in the telecommunication industry lies in the thermal range ($\lambda=1.54$ $\mu$m). The typical lattice parameters in the copolymer cubic phases are of the order of 30–100 nm.[15,16] This is the reason why the polymer based

 

structures obtain less experimental attention than colloidal systems. However, to be able to operate on the telecommunication frequency, photonic crystal should have domain sizes in the periodic structure of the order of 250 nm (Ref. 17) and such scale has been already obtained in block copolymers.[18] Moreover, on the basis of the block copolymers 1D, 2D, and 3D photonic crystals have already been made.[19]

Since the TPMCA display very interesting photonic properties we believe that it is important to know into which directions experimental efforts to fabricate them at the desired scale should follow.

The article is organized as follows. First we give a very brief introduction to the triply periodic minimal surfaces. In the next section we describe modeling of TPMCA. In Sec. IV we briefly outline the details of computations. Sections V and VI include the results for the 2V (two subvolumes, i.e., bicontinuous), 3V (three subvolumes, i.e., tricontinuous), and 4V and 5V TPMCA's based on balanced ($P$, $D$, $G$) and unbalanced [$I$-$WP$, $F$-$RD$, and $C(P)$] minimal surfaces, respectively. In Sec. VII we discuss PBG width dependence on the dielectric contrast for structures for which the widest PBG was found. The last section contains a summary of the results and outlook.

## II. PERIODIC SURFACES AND MULTIPLY CONTINUOUS STRUCTURES

The periodic surface is the surface that moves onto itself under a unit translation in one, two, or three coordinate directions similarly as in the periodic arrangement of atoms in regular crystals. The most interesting are triply periodic surfaces which are periodic in all three dimensions forming structures which have various crystallographic symmetries (Fig. 1).

The paradigm structures for all periodic surfaces are triply periodic minimal surfaces. The name minimal follows from the experiment of Plateau (Belgian physicist XIX century): use a soap solution and dip a metal frame (not necessarily planar) in it. The film that forms on the frame will adopt the shape such as to minimize the surface free energy, i.e., as to minimize the area of the surface (hence the name minimal surface). Moreover, from the minimization of the area it follows that the mean curvature of such a surface at every point is zero. So the name minimal surfaces have been adopted for all surfaces having zero mean curvature at every point.

Surfaces are characterized locally by the Gaussian $K$ and mean $H$ curvatures. $K$ and $H$ are given by the equations $H=1/2(1/R_1+1/R_2)$, $K=1/(R_1R_2)$, where $R_1$ and $R_2$ are the principal radii of curvature. The four typical surface motifs are spherical ($H>0$, $K>0$), cylindrical ($H>0$,$K=0$), planar ($H=0$,$K=0$), and a perfect saddle ($K<0$,$H=0$). The minimal surfaces consists of the perfect saddles, i.e., their mean curvature $H=0$ at every point. The unit cells of some of the triply periodic minimal surfaces (TPMS's) are shown in Fig. 1.

The periodic surface divides the volume into two congruent non-intersecting subvolumes. Each of the subvolumes forms a continuous network inside the whole system. Since

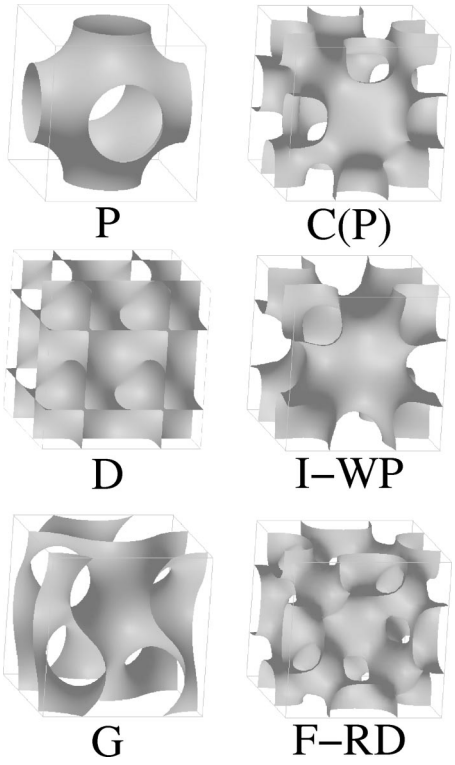


FIG. 1. The unit cells of the triply periodic minimal surfaces studied in this paper.

there are two such continuous (percolating) subvolumes the structure is called bicontinuous. One can imagine a more complex situation when there are two triply periodic surfaces inside the system (Fig. 2). They divide the space into three congruent nonintersecting subvolumes and hence such structure is called tricontinuous. In general one can consider $n$ periodic surfaces separating a space into $n+1$ congruent nonintersecting subvolumes.

Such structures are formed in surfactant systems, diblock copolymers, ionic crystals, etc.[20] In order to illustrate the formation of such structures in real systems let us consider

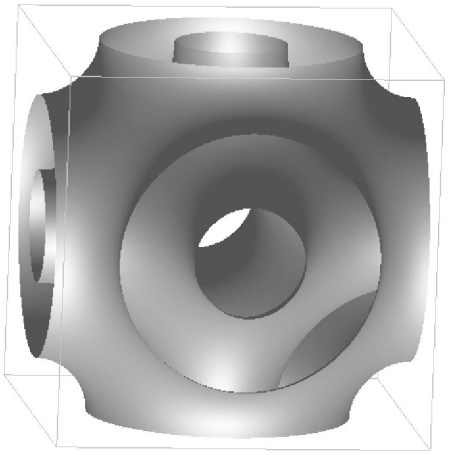

FIG. 2. The example of the unit cell of the tricontinuous periodic system. Two triply periodic surfaces divide space into the three congruent nonintersecting subvolumes.

the case of diblock copolymers. An *A*-*B* diblock copolymer is a polymer consisting of a linear sequence of *A*-type monomers chemically joined to a sequence of *B*-type monomers. Even a small amount of incompatibility (difference in interactions) between monomers *A* and monomers *B* can induce phase separation. However the *A* and *B* homopolymers are chemically joined in a diblock, therefore a system of diblocks cannot undergo a macroscopic phase separation. Instead a number of order-disorder phase transitions take place in the system between the isotropic phase and spatially ordered phases in which *A*-rich and *B*-rich domains, of the size of a diblock copolymer are arranged in a periodic way. The surface in this case is defined as the average location of the chemical bonding between the *A* homopolymer and *B* homopolymer. Among the structures formed by the *A*-*B* diblock copolymer there are bicontinuous structures where the surface between continuous *A*-rich subvolume and *B*-rich subvolume is the triply periodic surface such as one of those shown in Fig. 1. A number of possible triply periodic minimal surfaces is infinite and it has been recently shown that they can be generated as the local minima of the Landau-Ginzburg functional used to describe ordering phenomena in microemulsion.[21]

## III. MODELING OF THE MULTICONTINUOUS TRIPLY PERIODIC ARCHITECTURES

The TPMCA are composed of continuous subvolumes which are interwoven but distinct. The surfaces which divide the different continuous domains are triply periodic surfaces which can be derived from the triply periodic minimal surfaces (Fig. 1). They can be modeled by the constant mean curvature (CMC) surfaces or parallel surfaces (PS). These two approaches are very close to each other and lead to a close agreement in various calculated properties.[22–25] In our work we have used the PS as they are easier to handle. The construction of the PS is shown and described in Fig. 3.

The base TPMS divides the volume of the unit cell into two subvolumes. In the case of the balanced TPMS the two systems of channels have the same volume fraction and are identical and can be transformed onto each other by the operation from the appropriate space symmetry group. Still we can orient the TPMS and obtain an unambiguous distinction of the channels. One of them can be called a negative channel and the other a positive one. Then if we shift the base TPMS by a negative displacement we shrink the negative channel and expand the positive one. Each channel is associated with a construction made out of straight rods which join at a given coordination number (Fig. 4). The skeletal networks are only an abstract geometrical constructions which are not really present in the system.

In the case of only one interface PS there are only two distinct channels each containing it's skeletal core. To compute the dispersion relations $\omega(\mathbf{k})$ we have assigned one of the channels with a high dielectric constant (DC) and the other one with a low DC. Thus the structure is composed of a single dielectric network in an air matrix. This situation is schematically shown in the top panel of Fig. 5. The volume fraction of the dielectric channel $\phi_{\mathrm{ch}}$ can be adjusted by

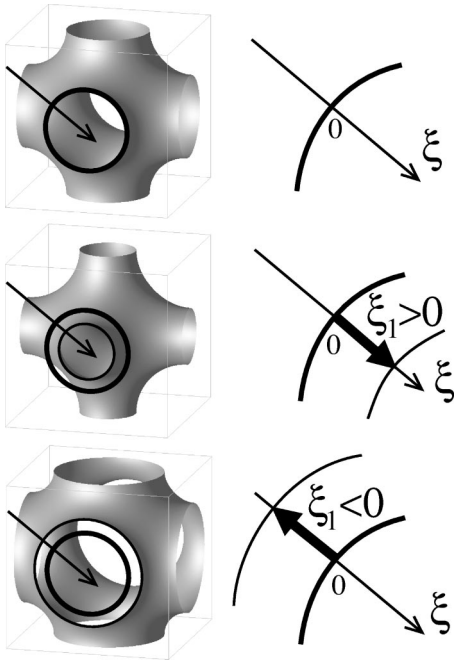


FIG. 3. The construction of the constant distance parallel surfaces (PS). In every point of the TPMS (top panel) an axis $\xi$ normal to it can be drawn and oriented into one of the subvolumes into which the TPMS divides the space. If we mark a given displacement $\xi_1$ on every $\xi$ axis and stretch a surface through resultant points we obtain a PS. When $\xi_1$ is positive we shrink the plus network (middle panel) and when $\xi_1$ is negative we shrink the minus network (bottom panel).

shifting the PS. For the TPMCA's based on the balanced TPMS there is a symmetry between the positive and negative skeletal cores. Therefore an inverse situation (obtained by interchanging the skeletal networks) does not have to be considered.

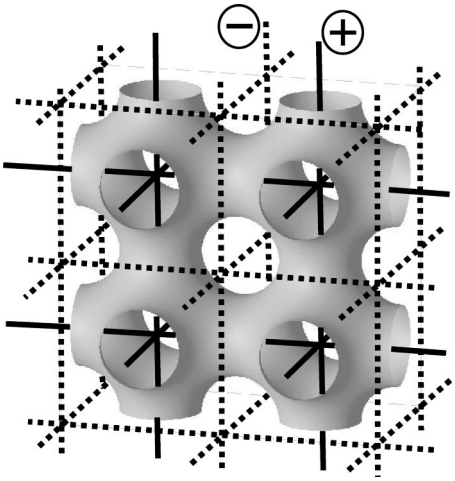


FIG. 4. Each TPMS divides the space into two distinct networks. Each of them can be represented by a skeletal core consisting of straight rods joining at given coordination numbers. In the case of the balanced TPMS both cores are geometrically and topologically equivalent. Still one can assign a different name to each of them (here plus and minus). This distinction becomes important when unbalanced TPMS are taken into account.

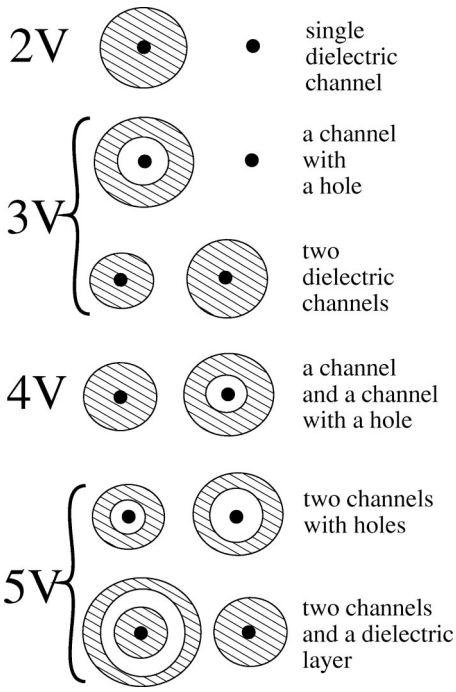


FIG. 5. An interpretation of the triply periodic multicontinuous architectures (TPMCA's). The black dots represent the abstract skeletal constructions around which either air or dielectric channels are created. In the case of the unbalanced templates the cores should be assigned with the plus/minus signs and their inversion changes the structure. See Sec. III for explanation.

Building a three subvolume structure results in a network containing (i) the negative core, (ii) a layer around it, and (iii) a network with the positive core inside. In this case there are two possible ways to assign the dielectric constants. One is to create two dielectric networks separated by an air layer. Then we have two parameters defining the structure—the volume fractions of the first $\phi_{\mathrm{ch}(1)}$ and second channels $\phi_{\mathrm{ch}(2)}$. The other possibility is to put a hole in the dielectric network—then the parameters are the volume fraction of the channel $\phi_{\mathrm{ch}}$ (including the hole) and of the hole itself $\phi_h$. In fact the second possibility can be equivalently interpreted as two air networks with a dielectric layer between them. Both situations are schematically sketched in Fig. 5.

The four subvolume structure has three PS. Again in the case of the balanced templates the symmetry allows us to choose a convenient interpretation which is shown in Fig. 5. We will discuss the dependence of the band widths on three parameters $\{\phi_{\mathrm{ch}(1)},\phi_{\mathrm{ch}(2)},\phi_{h(2)}\}$.

Finally, the most complicated, five subvolume structure can be build in two ways. The first one has two pierced dielectric networks $\{\phi_{\mathrm{ch}(1)},\phi_{h(1)},\phi_{\mathrm{ch}(2)},\phi_{h(2)}\}$, the other has two dielectric networks separated by air, dielectric, and air layers $\{\phi_{\mathrm{ch}(1)},\phi_{\mathrm{air}(1)},\phi_{\mathrm{layer}},\phi_{\mathrm{ch}(2)}\}$.

## IV. COMPUTATIONS OF THE PHOTONIC BAND STRUCTURE

The photonic crystal is a periodic arrangement of regions with different dielectric constants $\epsilon$. The laws governing the propagation of electromagnetic waves in such a medium are given by ME. Ignoring the nonlinear effects, possible solutions of ME's can be expressed as a superposition of the time-harmonic modes. The frequencies of these modes are an eigenvalues of a linear Hermitian operator[26] forming discrete sequence of bands (''dispersion relations'') $\omega_n(\mathbf{k})$ as a functions of the ''wave vector'' $\mathbf{k}$. Note, that all the properties of the band structure are completely specified by specifying all the bands in the first Brillouin zone (BZ). Due to symmetries, one can further restrict values of $\mathbf{k}$, leading to different $\omega_n$, to the irreducible part of the first BZ. The space symmetry groups of the studied structures as well as the types of their reciprocal lattices are given in Table I.

TABLE I. Space symmetry groups and types of reciprocal lattice of the TPMCA based on various TPMS's (Ref. 27). sc: simple cubic, bcc: body centered cubic, fcc: face centered cubic.

| TPMS template | TPMCA space group | reciprocal lattice |
|---|---|---|
| $P$ | $Pm\bar{3}m$ (221) | sc |
| $D$ | $Fd\bar{3}m$ (227) | bcc |
| $G$ | $I4_132$ (214) | fcc |
| $C(P)$ | $Pm\bar{3}m$ (221) | sc |
| $I$-$WP$ | $Im\bar{3}m$ (229) | sc |
| $F$-$RD$ | $Fm\bar{3}m$ (225) | sc |

There are few common approaches to the eigendecomposition of ME's. Two most frequently used are frequency-domain or time-domain techniques. In the frequency-domain approach one expands the fields in some basis subjected to a finite truncation. Most often the plane-wave basis is used. Then a resulting linear eigenproblem is solved. The time-domain techniques involve direct simulations of ME over time on a discrete grid using finite-difference time-domain (FDTD) algorithms. The frequencies (band structure) are then extracted via a Fourier-transform of the fields.

Since we are primary interested in the photonic band structure of the TPMCA, the frequency-domain approach is the most natural choice. We have used a freely available MPB (Refs. 28 and 29) computation package to find fully vectorial eigenmodes of ME and the corresponding dispersion relations. The MPB uses smoothed effective dielectric tensor,[30] which brings convergence proportional to the square of spatial resolution even for sharply discontinuous dielectric structures. In our calculations we have modeled the unit cell with a resolutions 64, 128, and 256 in each of three dimensions with computational grid of size 32, 40, 48, 64, and stated expected convergence.

We performed closest point transform (CTP) of the TPMS, i.e., in each space point we computed minimal distance to the surface. Level surfaces of the resulting scalar field of distances are exactly the PS introduced above. They form the boundaries of the different DC domains.

We have investigated structures composed from only two kinds of material with distinct DC's—$\epsilon_{\mathrm{low}}$ and $\epsilon_{\mathrm{high}}$, respectively. In the search for the widest PBG we have used $\epsilon_{\mathrm{low}}=1$ and $\epsilon_{\mathrm{high}}=13$. Only for the ''champion'' structures the

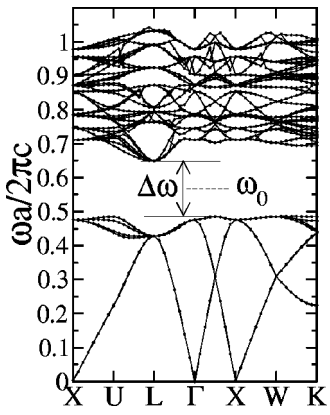


FIG. 6. The dispersion relations $\omega_n(\mathbf{k})$ ($n \leqslant 55$) for the double diamond dielectric network ($\epsilon_{\text{high}}=13$) of a volume fraction $\phi_{\text{ch}}=0.23$ in an air matrix ($\epsilon_{\text{low}}=1$). The relative width of the complete photonic band gap of this structure reaches a remarkably high value of $f=100(\Delta\omega/\omega_0)=28.7$. Here $\Delta\omega=\omega_{\text{top}}-\omega_{\text{bottom}}$ is the difference between the lower limit $\omega_{\text{top}}$ of the frequency of the bands above and upper limit $\omega_{\text{bottom}}$ of the bands below the gap. The middle frequency $\omega_0$ is the average of $\omega_{\text{top}}$ and $\omega_{\text{bottom}}$. All of the frequencies are given in the units of $2\pi c/a$ where $a$ is the lattice parameter of the structure. The unit cell of this champion architecture is visualized in Fig. 7.

dependence on the dielectric contrast is discussed in Sec. VII. The *P*, *D*, *G* and *I-WP* triply periodic minimal surfaces (TPMS's) have been approximated by the new, efficient from computational viewpoint, improved nodal approximations taken from Ref. 31 and the *F-RD* and *C*(*P*) from Ref. 27.

## V. RESULTS: BALANCED TPMS TEMPLATES

### A. *D*: Double diamond TPMCA family

The two subvolume (2V) structures are composed of a single dielectric network in an air matrix. For the preliminary runs we have set the DC of the network $\epsilon_{\text{high}}=13.0$. Now the only variable left is the volume fraction $\phi_{\text{ch}}$ of the dielectric channels. In the first step the structures were sampled with an increment $\Delta\phi_{\text{ch}}=0.1$. Then a finer $\phi_{\text{ch}}$ grid was imposed. All together 39 different D2V structures have been explored. The dispersion relations $\omega_n(\mathbf{k})$ have been computed up to the $n=55$ band. In addition to the gap between the eighth and ninth band (8-9) also a (32-33) gap has been noticed for $\phi_{\text{ch}}=0.3$ with $f<1$. The latter one is, perhaps, of little practical importance because of very small width and high position in the spectrum. It's technological exploration will require very accurate reproducing of the structure, which seems problematic (or impossible at all). The QF of the (8-9) PBG reaches the largest value of 28.7 for $\phi_{\text{ch}}=0.23$. The corresponding dispersion relation diagram is shown in Fig. 6 and the structure itself in Fig. 7. The dependence of the (8-9) gap on $\phi_{\text{ch}}$ is shown in Fig. 8.

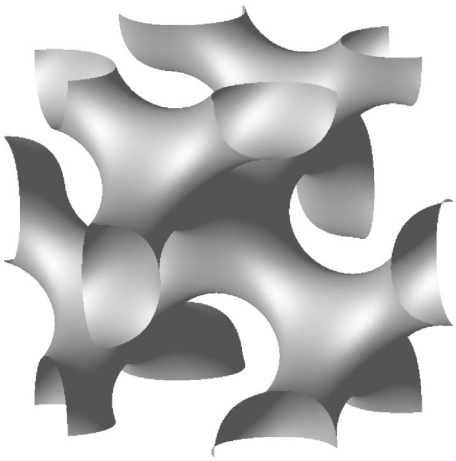

FIG. 7. The unit cell of the structure exhibiting the largest complete photonic band gap out of all the structures studied here. Corresponding dispersion relations are shown in Fig. 6.

The three subvolume (3V) binary DC structures can be built in two possible ways. One is to assign the high DC to the subvolume in the middle of the structure. This results in the dielectric channel surrounded with the hollow channels architectures. The second possibility is to keep the middle subvolume with a low DC which makes two dielectric channels with the hollow in between. In both cases there are two adjustable parameters which can be varied: $\{\phi_{\text{ch}},\phi_h\}$ and $\{\phi_{\text{ch}(1)},\phi_{\text{ch}(2)}\}$, respectively. In the preliminary runs both variables have been sampled with $\Delta\phi=0.05$ increment. In interesting regions finer $\phi$ grid has been implemented. All together 121 structures have been sampled. Contrary to Maldovan *et al.*[14] we find that both kinds of D3V structures display full 3D PBG.

D3V: dielectric channel with a hole. In addition to the wide (8-9) gap which has been checked in detail also the (32-33) PBG has been observed. We found the largest QF values for two samples $f=4.0$ ($\phi_{\text{ch}}=0.35,\phi_h=0.15$) and $f=3.8$ for ($\phi_{\text{ch}}=0.4,\phi_h=0.1$). Still as it is much smaller then the (8-9) gap we did not look for the structures in which it would obtain the best QF. The dependence of the QF for (8-9) gap is shown in Fig. 8. Putting a hole throughout the dielectric network does not enhance the PBG. In fact the act

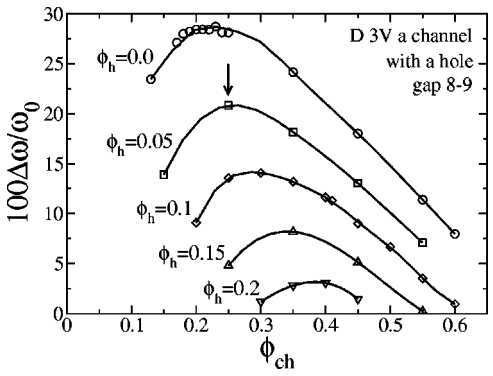


FIG. 8. The relative width of the (8-9) photonic band gap as a function of the channel volume fraction $\phi_{\text{ch}}$ in the D 3V pierced dielectric network structure, i.e., the network with a single dielectric channel of volume fraction $\phi_{\text{ch}}$ pierced in the middle by the hollow channel of the volume fraction $\phi_h$ (see Fig. 4). Different curves correspond to the different values of $\phi_h$. Top panel of Fig. 9 shows, as an example, one of those structures for $\phi_{\text{ch}}=0.25$, $\phi_h=0.05$ indicated by an arrow on this plot.

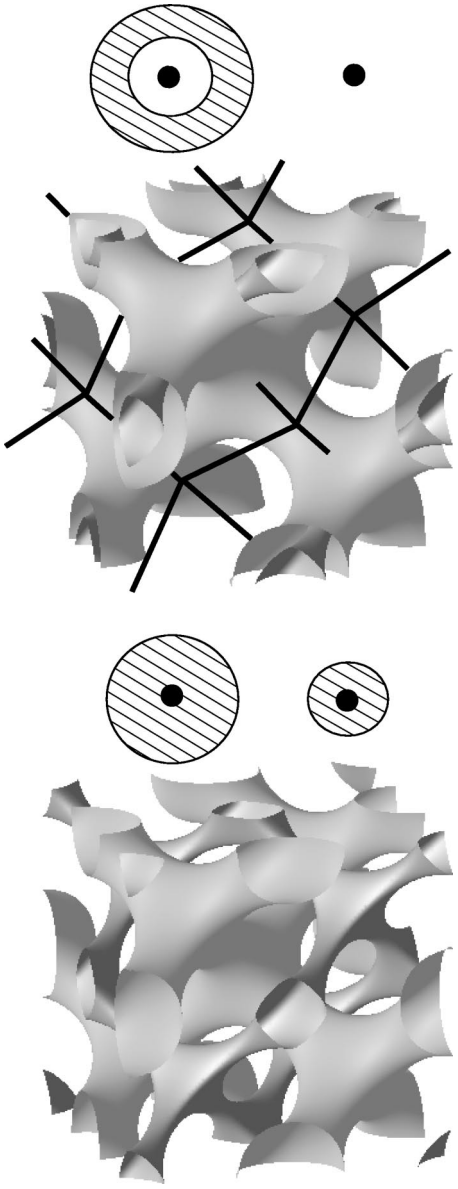

FIG. 9. The *D* 3V structures. Upper panel presents a *pierced dielectric network* architecture. The network is built around one of the skelets while the other side remains empty. The solid lines show the second skeletal network. The second possibility of the two dielectric networks is shown in the bottom panel. Here a dielectric network is built around each of the cores.

of perforation of the dielectric network could be interpreted as a perturbation to the otherwise perfect 2V architecture. The widest (8-9) PBG 3V structure (out of the ones tested) is visualized in the upper panel of Fig. 9.

D3V: two dielectric networks. Only the (8-9) PBG has been observed. The (8-9) QF's are sketched in Fig. 10. Again introducing another dielectric domain to a 2V structure only weakens the gap. It is worth noting here that the gap closes up completely for $\phi_{\mathrm{ch}(1)}=\phi_{\mathrm{ch}(2)}$—that is, for the symmetric structures. This explains why Maldovan *et al.*[14] did not see any gaps at all, as they probably tested only symmetric 3V structures. The architecture for which the widest (8-9) PBG was observed is shown in the bottom of Fig. 9.

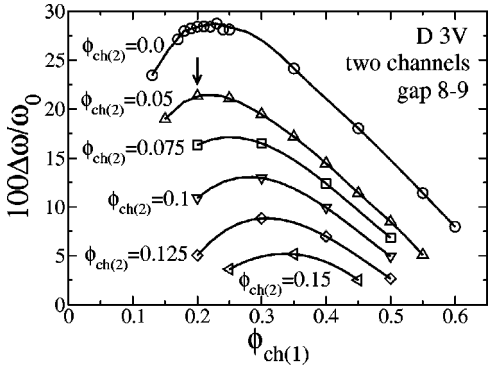


FIG. 10. The relative width of the (8-9) photonic band gap as a function of the channel volume fraction $\phi_{ch(1)}$ in the *D* 3V two dielectric network structure, i.e., the network with two dielectric channels of volume fractions $\phi_{\mathrm{ch}(1)}$ and $\phi_{\mathrm{ch}(2)}$ with a hollow channel of volume fraction $1-\phi_{\mathrm{ch}(1)}-\phi_{\mathrm{ch}(2)}$ in between (see Fig. 4). Different curves correspond to the different values of $\phi_{\mathrm{ch}(2)}$. The bottom panel of the Fig. 9 shows, as an example, one of those structures for $\phi_{\mathrm{ch}(1)}=0.2$, $\phi_{\mathrm{ch}(2)}=0.05$ indicated by an arrow on this plot.

The four subvolume (4V) *D* based TPMCA's have been sampled with $\Delta\phi=0.1$. The parameters subjected to variation were the first dielectric network volume fraction $\phi_{\mathrm{ch}(1)}$, the second network $\phi_{\mathrm{ch}(2)}$ (including the hole), and the air hole's volume fraction $\phi_h$. Taking into account the $(+,-)$ symmetry these results in 84 different structures. The (8-9) PBG has a smaller width than the one for the 2V systems. The results for the nonzero (8-9) PBG D4V structures are shown in Fig. 11. The largest QF value ($f=21.6$) was found for ($\phi_{\mathrm{ch}(1)}=0.2$, $\phi_{\mathrm{ch}(2)}=0.7$, and $\phi_h=0.6$). The general tendency is that the bigger the second network and it's air hole the wider the (8-9) PBG. In other words within the D4V structures the widest gaps are offered by a single dielectric network and a thin dielectric layer. The only other PBG found was again the (32-33) gap with the best QF approaching 2.1 for the ($\phi_{\mathrm{ch}(1)}=0.1$, $\phi_{\mathrm{ch}(2)}=0.8$, and $\phi_h=0.6$) sample.

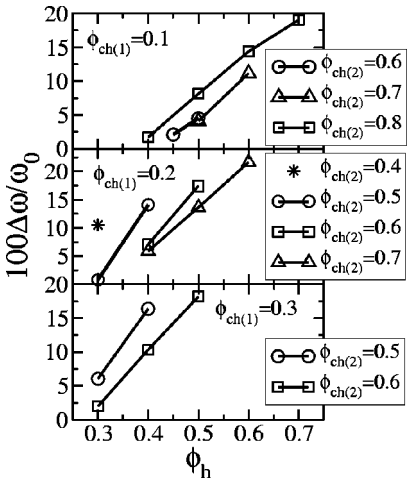


FIG. 11. The relative width of the (8-9) photonic band gap for the *D* 4V network and a pierced network structures (see text and Fig. 4 for explanation of the dielectric architecture).

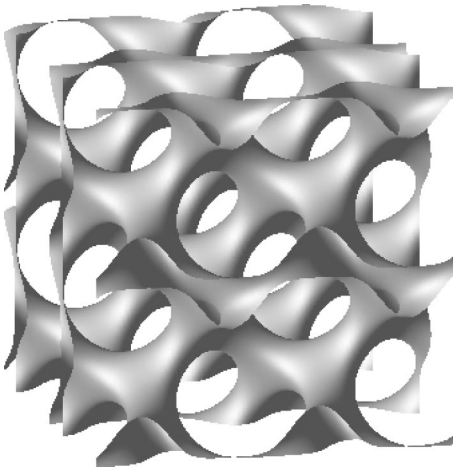

FIG. 12. Eight unit cells of the champion gyroid architecture (see Fig. 13).

**The five subvolume** (5V) D based structures did not exhibit significant gaps. The structures have been sampled with $\Delta\phi=0.11$ (78 structures tested). In the range of the parameters studied we have found only (8-9) gaps for the architectures composed of two dielectric networks separated by an air, dielectric and air layers. The (8-9) QF obtained the largest value of $f=6.8$ for ($\phi_{ch(1)}=0.11$, $\phi_{air(1)}=0.11$, $\phi_{layer}=0.11$ and $\phi_{ch(2)}=0.34$). In the case of the two pierced dielectric networks the (8-9) QF has reached a similar value $f=6.2$ ($\phi_{ch(1)}=0.22$, $\phi_{h(1)}=0.11$, $\phi_{ch(2)}=0.67$ and $\phi_{h(2)}=0.56$).

### B. *G*: Gyroid TPMCA family

**G2V** The preliminary increment was $\Delta\phi=0.1$. However together 99 G2V structures have been tested. The widest is the (4-5) gap which acquires the QF 26.6 for $\phi_{ch}=0.19$. This structure is visualized in Fig. 12. The whole dependence of the (4-5) gap width on the volume fraction of the dielectric network is shown in Fig. 13. Apart from the (4-5) PBG only a (36-37) pseudogap has been observed for $0.35<\phi_{\rm ch}<0.45$.

128 three subvolume gyroid structures were tested with the starting $\phi$ increment $\Delta\phi=0.05$ and then finer grid applied. Again the structures can be divided into two classes.

G3V: a perforated dielectric network. As in the case of the D3V structures, the G3V display weaker gaps than the 2V samples. Increasing the volume of an air hole in the dielectric channel causes a systematic closing up of the (4-5) PBG. This is illustrated in Fig. 13. Apart from the (4-5) gap three other small PBG have been found. The (16-17) gap opens up for $\phi_{\rm ch}\in(0.4,0.8)$ and $\phi_h\in(0.1,0.3)$. It acquires the largest QF value of 1.4 in the ($\phi_{\rm ch}=0.6$ and $\phi_h=0.3$) sample. The ($\phi_{\rm ch}=0.3$ and $\phi_h=0.1$) structure opens up a (28-29) PBG ($f\approx1$). Finally two (40-41) gaps have been observed: $f\approx1$ ($\phi_{\rm ch}=0.4$ and $\phi_h=0.1$) and $f=1.2$ ($\phi_{\rm ch}=0.5$ and $\phi_h=0.1$). These gaps are too small to be significant for the applications.

G3V: two dielectric networks. Again, as in the case of D3V, introducing the second dielectric network in the 2V

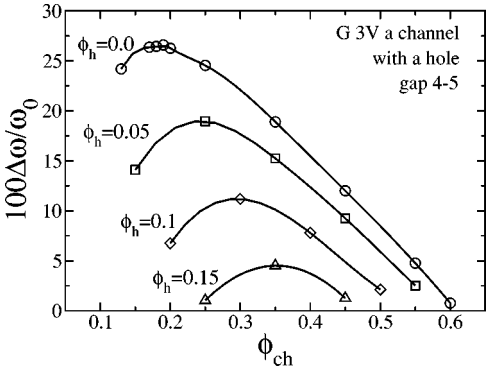


FIG. 13. The relative width of the (4-5) photonic band gap as a function of the channel volume fraction $\phi_{\rm ch}$ in the *G* 3V pierced dielectric network, i.e., the network with a single dielectric channel of volume fraction $\phi_{\rm ch}$ pierced in the middle by the hollow channel of the volume fraction $\phi_h$ (see Fig. 4). Different curves correspond to the different values of $\phi_h$. A curve for the 2V structure (no hole, $\phi_h=0$) is shown for comparison. The best 2V structure ($f=26.6$ for $\phi_{ch}=0.19$) is shown in Fig. 12.

structure only weakens the widest (4-5) gap (see Fig. 14). The larger the second network is the thinner the PBG is found. The (24-25) gap has been observed in the symmetric ($\phi_{\rm ch(1)}=0.1$ and $\phi_{\rm ch(2)}=0.1$) sample ($f\approx1$). In symmetric samples also the (8-9) pseudogap can be found for $[\phi_{\rm ch(1)},\phi_{\rm ch(2)}\in(0.1,0.15)]$. At $[\phi_{\rm ch(1)}=0.1$ and $\phi_{\rm ch(2)}\in(0.3,0.35)]$ a (36-37) gap opens up reaching $f<1$. These gaps are also insignificant.

G4V. The $\{\phi_{\rm ch(1)},\phi_{\rm ch(2)},\phi_{h(2)}\}$ structures have been sampled with $\Delta\phi=0.1$ resolution. The widest is again the (4-5) PBG. It's width dependence on the structural parameters is shown in Fig. 15. Similarly to the D4V structures the widest (4-5) gaps are found for large values of $\phi_{\rm ch(2)}$ and $\phi_h(2)$—that is, for a single dielectric network and a thin dielectric layer. Apart from the (4-5) gap few other have been observed. The most commonly found is a very weak (16-17)

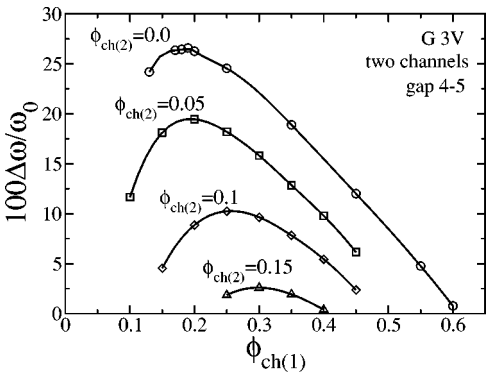


FIG. 14. The relative width of the (4-5) photonic band gap as a function of the channel volume fraction $\phi_{\rm ch(1)}$ in the *G* 3V two dielectric network structure, i.e., the network with two dielectric channels of volume fractions $\phi_{\rm ch(1)}$ and $\phi_{\rm ch(2)}$ with a hollow channel of volume fraction $1-\phi_{\rm ch(1)}-\phi_{\rm ch(2)}$ in between (see Fig. 4). Different curves correspond to the different values of $\phi_{\rm ch(2)}$. A curve for the 2V structure (without the second channel, $\phi_{\rm ch(2)}=0$) is shown for comparison.

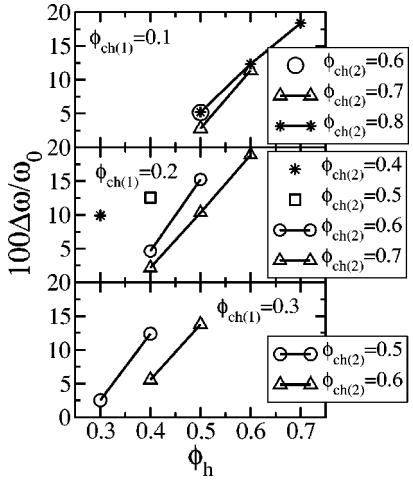


FIG. 15. The relative width of the (4-5) photonic band gap of the *G* 4V a network and a pierced network structures (see text and Fig. 4 for explanation of the dielectric architecture).

PBG with the QF approaching the value of 1.2 ($\phi_{ch(1)}=0.1$, $\phi_{ch(2)}=0.7$, and $\phi_{h(2)}=0.3$). Also (32-33) $f\approx 1$ gap has been found ($\phi_{ch(1)}=0.1$, $\phi_{ch(2)}=0.7$, and $\phi_{h(2)}=0.4$). Pseudogaps (28-29), (34-35), and (42-43) occasionally appear. Apart for 4-5 gap no other significant gaps have been found.

G5V: two perforated dielectric networks. The widest is again gap (4-5) reaching $f=2.5$ for ($\phi_{ch(1)}=0.22$, $\phi_{h(1)}=0.11$, $\phi_{ch(2)}=0.56$, and $\phi_{h(2)}=0.45$). Gap (16-17) obtains similarly small QF value $f=1.3$ at $\phi_{ch(1)}=0.33$, $\phi_{h(1)}=0.22$, $\phi_{ch(2)}=0.56$, and $\phi_{h(2)}=0.34$). Also (28-29), (32-33), (40-41), and (42-43) pseudogaps have been found, which have no significance from the practical point of view.

G5V: two dielectric networks and a dielectric layer. (4-5) PBG has been observed in only one sample with $f=3.2$ ($\phi_{ch(1)}=0.11$, $\phi_{air(1)}=0.44$, $\phi_{layer}=0.11$, and $\phi_{ch(2)}=23$). In two samples also weak (16-17) and (48-49) PBG were found. As in the case of D5V these results did not prompt us to test more than the initial 78 structures.

### C. *P*: Plumber's nightmare TPMCA family

For all 2V, 3V, and 4V TPMCA's based on *P* TPMS tested (187 structures) the widest is the (5-6) PBG. It acquires the largest QF value $f=11.2$ for a 2V architecture with $\phi_{ch}=0.22$. Introducing additional air/dielectric subvolumes decreases the gap width. The nonzero (5-6) gap results are sketched in Fig. 16. Apart from the (5-6) PBG only four others have been found. (11-12) and (38-39) gaps with $f=3.6$ and $f\approx 1$, respectively, in a symmetric P3V ($\phi_{ch(1)}=\phi_{ch(2)}=0.1$) sample. Two gaps in a P3V pierced dielectric network structure: (19-20) $f=1.1$ ($\phi_{ch}=0.3$, $\phi_h=0.1$) and (28-29) pseudogap ($\phi_{ch}=0.6$, $\phi_h=0.2$). The 4V structures tested did not exhibit any gap in addition to the (5-6) one. The 5V *P* TPMCA have not been sampled.

## VI. RESULTS: UNBALANCED TPMS TEMPLATES

For the TPMCA based on unbalanced TPMS there is no symmetry between the plus and minus networks of channels.

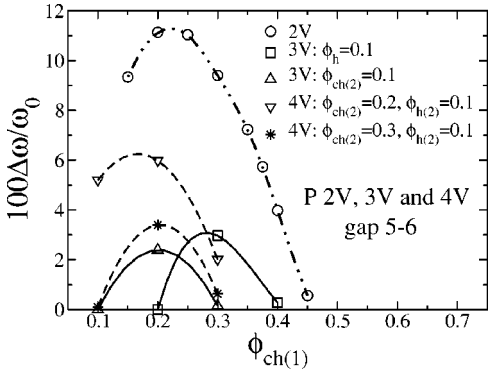


FIG. 16. The relative width of the (5-6) photonic band gap of the various TPMCA's based on the Plumber's nightmare TPMS (see text and Fig. 4 for explanation of the dielectric architecture).

For example in the case of an *I-WP* based 2V structure the minus network is four coordinated and the plus channels are eight coordinated. Therefore even a single dielectric network which originates from the minus core is a different structure than a network originating from the plus core. In general these two structures can have different photonic properties. This lack of symmetry has been taken into account in testing the *I-WP*, *F-RD*, and *C*(*P*) based TPMCA's. Still as they open only weak gaps or do not open complete PBG at all we will not discuss their construction in detail. An interested reader can find such a description in Ref. 25.

For the *C*(*P*)-Neovious, conjugate to *P*-TPMCA family we have found only a (19-20) pseudogap in 2V structures. The 4V and 5V architectures have not been sampled.

The *F-RD*-TPMCA family did not exhibit any gaps at all in the range (only 2V) of the structures tested. Since in the case of *P*, *D*, and *G* TPMS based families the largest PBG's have been found in 2V architectures, we did not sample any more complicated structures.

*I-WP* wrapped package TPMCA family. The 2V and 3V TPMCA's did not present any gaps at all. In the 4V samples we have found two pseudo gaps (18-19) and (46-47). The 5V structures have not been tested.

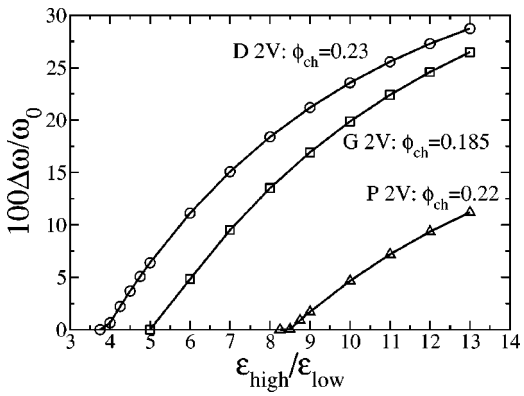


FIG. 17. The dependence of the relative width of the photonic band gap on the dielectric contrast for the champion *D*, *G*, and *P* 2V structures.

## VII. DC CONTRAST

In the last two sections we have been investigating the dependence of the PBG widths on the structure of the TPMCA. For this purpose we have set the DC contrast to $\epsilon_{high}/\epsilon_{low}$. Now we want check what is the lowest contrast in which the widest gap are still exhibited. For this reason we have computed the band spectra for various DC contrasts. The results for the champion structures are shown in Fig. 17.

It is worth noting that the (8-9) complete PBG in the double diamond 2V structure has a significant width ($f=11.1$) for the DC contrast as low as $\epsilon_{high}/\epsilon_{low}=6$. Such a contrast can be realized in the inorganic-organic hybrid materials with a semiconductor material $\epsilon_{high}>12$ and a polymer matrix $\epsilon_{low}\approx 2$.

## VIII. CONCLUSIONS

(i) In the case of the TPMCA's based on balanced TPMS's the widest gaps are found for the simplest, two subvolume structures. The D2V and G2V architectures present very wide complete PBG which persist down to the DC contrast as low as $\epsilon_{high}/\epsilon_{low}\approx 6$.

(ii) The TPMCAS based on unbalanced *I-WP*, *F-RD*, and *C(P)* TPMS did not present any significant complete PBG. Of course it does not justify a conclusion that the symmetry of channels into which the TPMS divides the space is a condition for opening a complete gap.

(iii) In the range of parameters studied the multichannel (4V, 5V) architectures did not enhance nor the gap width neither they did open the multiple gaps.

## ACKNOWLEDGMENTS

This work was supported by the KBN Grant No. 2P03B00923. P.G. acknowledges support from the Foundation for Polish Science (FNP).

*Present address: Department of Chemistry and Chemical Biology Department, Harvard University, 12 Oxford Street, Cambridge, MA 02138.

[1] E. Yablonovitch, Phys. Rev. Lett. **58**, 2059 (1987).
[2] S. John, Phys. Rev. Lett. **58**, 2486 (1987).
[3] K.M. Ho, C.T. Chan, and C.M. Soukoulis, Phys. Rev. Lett. **65**, 3152 (1990).
[4] L. Zavieh and T.S. Mayer, Appl. Phys. Lett. **75**, 2533 (1999).
[5] M. Francois *et al.* Microelectron. Eng. **61**, 537 (2002).
[6] D.M. Dabbs and I.A. Aksay, Annu. Rev. Phys. Chem. **51**, 601 (2000).
[7] O.D. Velev, P.M. Tessier, A.M. Lenhoff, and E.W. Kaler, Nature (London) **401**, 548 (1999).
[8] S.R.J. Oliver, T.D. Clark, N. Bowden, and G.M. Whitesides, J. Am. Chem. Soc. **123**, 8119 (2001).
[9] P. Alexandridis, U. Olsson, and B. Lindman, Langmuir **13**, 23 (1997).
[10] P.F.W. Simon *et al.* Comput. Mater. Sci. **13**, 3464 (2001).
[11] E. Velasco, L. Mederos, and G. Navascues, Langmuir **14**, 5652 (1998).
[12] J.F. Bertone, P. Jiang, K.S. Hwang, D.M. Mittleman, and V.L. Colvin, Phys. Rev. Lett. **83**, 300 (1999).
[13] L. Martín-Moreno, F.J. García-Vidal, and A.M. Somoza, Phys. Rev. Lett. **83**, 73 (1999).
[14] M. Maldovan, A.M. Urbas, N. Yufa, W.C. Carter, and E.L. Thomas, Phys. Rev. B **65**, 165123 (2002).
[15] J. Suzuki, M. Seki, and Y. Matsushita, J. Chem. Phys. **112**, 4862 (2000).
[16] T.A. Shefelbine, M.E. Vigild, M.W. Matsen, D.A. Hajduk, M.A. Hillmyer, E.L. Cussler, and F.S. Bates, J. Am. Chem. Soc. **121**, 8457 (1999).
[17] Y. Fink, J.N. Winn, S.H. Fan, C.P. Chen, J. Mitchel, J.D. Joannopoulos, and E.L. Thomas, Science **282**, 1679 (1998).
[18] A.C. Edrington, A.M. Urbas, P. DeRege, C.X. Chen, T.M. Swager, N. Hadjichristids, M. Xenidou, L.J. Fetters, J.D. Joannopoulos, Y. Fink, and E.L. Thomas, Adv. Mater. **13**, 421 (2001).
[19] Y. Fink, A.M. Urbas, M.G. Bawendi, J.D. Joannopoulos, and E.L. Thomas, J. Lightwave Technol. **17**, 1963 (1999).
[20] J. Klinowski, A.L. Mackay, and H. Terrones, Philos. Trans. R. Soc. London, Ser. A **354**, 1975 (1996).
[21] W. Góźdź and R. Hołyst, Phys. Rev. E **54**, 5012 (1996).
[22] P.E. Harper and S.M. Grunner, Eur. Phys. J. E **2**, 217 (2000).
[23] D.M. Anderson, H.T. Davies, L.E. Scriven, and J.C.C. Nitsche, Adv. Chem. Phys. **77**, 337 (1990).
[24] P. Garstecki and R. Hołyst, Langmuir **18**, 2519 (2002).
[25] P. Garstecki and R. Hołyst (unpublished).
[26] J. D. Joannopoulos, R. D. Meade, and J. N. Winn, in *Photonic Crystals* (Princeton University Press, Princeton, 1995).
[27] U.S. Schwarz and G. Gompper, Phys. Rev. E **59**, 5528 (1999).
[28] S.G. Johnson and J.D. Joannopoulos, Opt. Express **8**, 173 (2001).
[29] URL http://ab-initio.mit.edu/mpb/
[30] R.D. Meade, A.M. Rappe, K.D. Brommer, J.D. Joannopoulos, and O.L. Alherhand, Phys. Rev. B **48**, 8434 (1993); S.G. Johnson, *ibid.* **55**, 15 942(E) (1997).
[31] Paul J.F. Gandy, Sonny Bardhan, Alan L. Mackay, and Jacek Klinowski, Chem. Phys. Lett. **336**, 187 (2001).